Automated Image Acquisition of Parasternal Long-Axis View with Robotic Echocardiography

Yuuki Shida, Souto Kumagai, Ryosuke Tsumura, *IEEE member,* Hiroyasu Iwata, *IEEE member*

***Abstract*— This study proposes a method for finding a parasternal long-axis view in echocardiography autonomously with a robotic ultrasound (US) system. In obtaining this view, it is necessary to avoid the ribs and lungs because they reduce the clarity of US image. Meanwhile, the anatomical position and size of the heart, lungs, and ribs differ between individuals, which makes it difficult to find the optimal position of the US probe. Our proposed system is comprised of the following three processes. First, an exhaustive scan of the chest wall region is performed. The position of the probe that allows the mitral valve to be centrally positioned is estimated based on this scan. Second, the probe is rotated once in the yaw direction while being fixed in that position. The yaw angle is estimated at a point parallel to the left ventricular longitudinal axis in the acquired images. Finally, the pitch angle of the probe is estimated so that the probe avoids the connection between the mitral valve and the papillary muscle and chordae. To validate the proposed method, we performed human trials with five healthy subjects and measured the detection rate of observation points used to evaluate the image quality of parasternal long-axis view. The result showed that the median detection rate of the observation points was 63.3 ± 5.3%, which implies that the proposed method is valid.**

I. Introduction

Heart disease is the world's leading cause of death from disease; 17.9 million people died from heart disease in the year 2019 [1]. The mortality rate for heart disease could be improved significantly by early detection and treatment. However, low-income countries provide insufficient medical care. With the aging of society, the number of deaths from heart disease is increasing in developed countries. For example, the mortality rate of heart disease is increasing year on year in Japan, which has the most aged population among developed countries [2].

Periodic health checkups using transthoracic echocardiography have been attracting attention for this situation. This is because transthoracic echocardiography is noninvasive and provides a highly accurate diagnosis. On the other hand, ultrasonography, including transthoracic echocardiography, is challenging to carry out. Physicians and technologists need to be highly skilled and experienced, and there is a shortage of personnel.

A wide variety of robotic assistive technologies for ultrasound (US) examinations have been developed to solve the above problems. These robots have focused on several applications, including carotid, liver, and fetal echocardiography, cardiac tamponade, and other generic targets [3]–[7]. There are several studies focusing on the robotic echocardiography [8], [9] and we developed a seated-style echocardiography robot (see **Fig. 1**) [10]. The advantage of our robot system is to perform the US scan with the patient in a seated position, thus the patient can be immediately released from the robot in the event of an emergency.

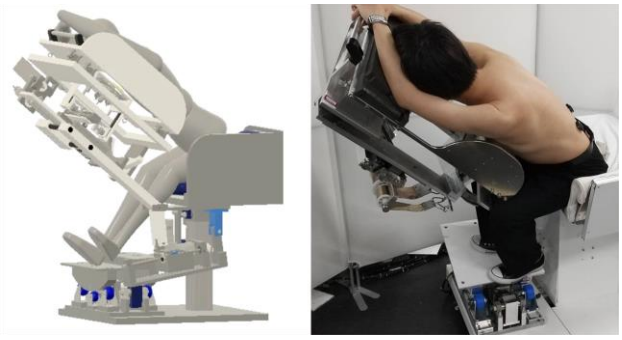

Fig.1. Seated-style echocardiography robot

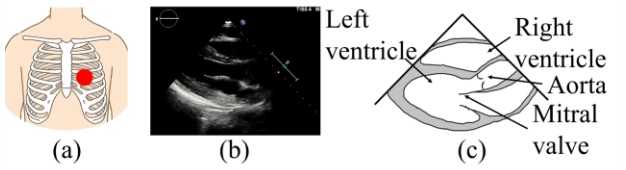

Fig.2. Parasternal long-axis view; (a) view acquisition position; (b) US image; (c) schematic depiction

Our ultimate goal is to automate echocardiography with the patient in the sitting position. Echocardiography requires comprehensive diagnosis using parasternal long- and short-axis views, an apical four-chamber view, and a subxiphoid view. To automate the echocardiography, the robot system needs to identify those views autonomously. As the first step for the automation, we focus on the parasternal long-axis view among the views in this study (see **Fig. 2**). The parasternal long-axis view is basically used to observe the presence or absence of an enlargement of the cardiac cavity, valve dynamics, and myocardial status. This allows the diagnosis of myocardial infarction, cardiomyopathy, valvular disease, and arrhythmia. To obtain this view, it is necessary to acquire the image from a position that avoids the lungs and costal bones, which reduce the clarity of the US image (hereafter referred to as the acoustic window). Meanwhile, the anatomical position and size of the heart, lungs, and ribs differ between individuals, which makes it difficult to find the optimal

*Research supported by the NSK Foundation for Advancement of Mechatronics and the Institute for Mechanical Engineering Frontiers.

Y. Shida and S. Kumagai are with the Graduate School of Creative Science and Engineering, Waseda University, Tokyo 169-8050, Japan (e-mail: yuuki-shida@iwata.mech.waseda.ac.jp)

R. Tsumura is with the Global Robot Academia Laboratory, Waseda University, Tokyo 169-8050, Japan (e-mail: r.tsumura2@kurenai.waseda.jp)

H. Iwata is with the Faculty of Science and Engineering, Waseda University, Tokyo 169-8050, Japan (e-mail: jubi@waseda.jp)

position of the acoustic position. In this study, we propose a method for estimating the acoustic window that allows the parasternal long-axis view to be acquired using the robot.

II. Related Works

In several previous studies, the diagnostic views were autonomously extracted from 3D volume data acquired by the physician through the acoustic window. Zhu et al. conducted a study to obtain six of the basic cross sections from physician-acquired 3D volume data that included the apex, right mitral valve, and left mitral valve [11]. Dong et al. proposed a method for left ventricular segmentation based on the FCN model [12]. Degel et al. proposed a method for left atrium segmentation using 3D US images [13]. Those studies assumed that the US probe was located on the acoustic window correctly, and that qualified image data were acquired. Meanwhile, in order to automate the procedure with the robot, it is necessary to locate the US probe in an appropriate position on the acoustic window. So far, many researches developed the autonomous robotic search method based on acquired US images, also known as visual servoing. Huang et al. and Nakadate et al. proposed a visual servoing method for the carotid artery, the first one is an exploration based on a procedure-specified imitation learning framework based on clinical protocols [14], and the latter one is an automated diagnostic system for the measurement of the wave intensity [15]. Zhou et al. developed a visual servo method for kidney using YOLOv5s and BiSeNet V2 [16]. Zielke et al combine a neural network-based segmentation with an automatic robotic ultrasound scanning for thyroid volumetry [17]. Jiang et al presented autonomous robotic scanning of US limbs using U-Net-type neural network [18]. However, no studies have focused on the visual servoing for the acoustic window of the heart by US imaging. The significant difference between the heart and other organs is that the heart position and shape change dynamically and drastically, which makes it difficult to search the target view compared to other organs. We believe that this is the first study for automating the acoustic window estimation by US imaging with the robot system in echocardiography.

III. Method

A. System Overview

In the proposed method, multiple US images obtained from the chest surface are analyzed in order to estimate the position and angle that enables the probe to acquire the parasternal long-axis view. The parasternal long-axis view is a view of the heart along the left ventricular long-axis. It is obtained by placing a probe between the third and fourth intercostal spaces (see **Fig. 2(a)**). The parasternal long-axis view should include the left ventricular outflow tract, aortic valve, mitral valve, and interventricular septum in the image. The interventricular septum is parallel to the parasternal long-axis, and the left ventricular outflow tract to the aortic valve is depicted in the parasternal long-axis view. Moreover, the mitral valve should be clear and not connected to the chordae and papillary muscle [19]. Our method estimates the acoustic window that satisfies the conditions for the delineation of the parasternal long-axis view based on these conditions.

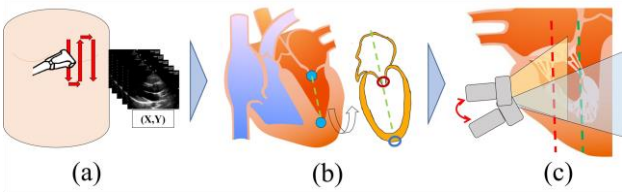

Fig.3. Schematic of the search method for the parasternal long-axis view; (a) mitral valve location search; (b) left ventricular long-axis angle search; (c) mitral valve angle search

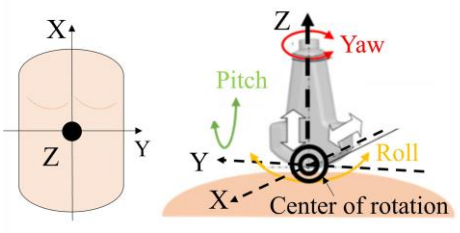

Fig.4 Degrees of freedom of US probe in the robot coordinate system

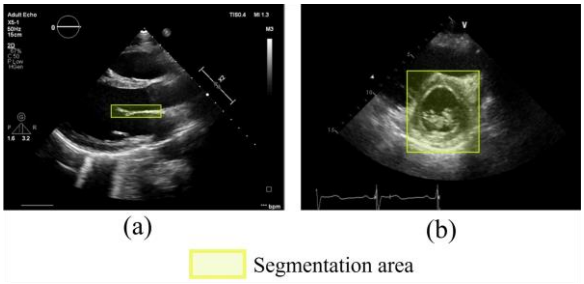

Fig.5. Example of annotation of the object detection model (a) mitral valve (b) the left ventricular region in the parasternal short-axis view at the level of the mitral valve

The system consists of three parts: i) mitral valve position search by positioning the probe along the x- and y-axes, ii) left ventricular long-axis angle search by rotating the probe in the yaw direction, and iii) mitral valve angle search by rotating the probe in the pitch direction. A schematic of the system is shown in **Fig. 3** Note that the degrees of freedom of the probe motion are defined as shown in **Fig. 4** in this paper. Roll, pitch and yaw angles correspond to the rotation angles of X-, Y- and Z-axes, respectively. The roll angle was fixed to 0° for this method.

B. Step 1: Mitral Valve Position Search

The goal of step 1 is to estimate the position (along the x- and y-axes) where the mitral valve can be captured in the center of the US image. The parasternal long-axis view should show the mitral valve at the center. In this step, a comprehensive search of the chest wall region to ensure that the mitral valve is captured in the acquired images is first performed. This is because the position of the mitral valve depends on the position of the heart and varies between individuals. After that, the position of the probe that allows the mitral valve to be captured at the center of the image is estimated by this search. The mitral valve was detected using Yolo v7 [20], an object detection method based on a deep learning model. The mitral valve object detection model was

trained using 3279 images for training and 820 images for validation. Images for training and validation were obtained from 7 males in their 20s. These images were acquired by adjusting the position and angle of the probe by hand and fulfilled the conditions for the parasternal long-axis view shown in **Fig. 2**. Annotation of mitral valves that were not fully closed in the training images was performed as shown in **Fig.5(a).** The number of epochs was 200 and batch size was 8. The mean average precision 50 (mAP50) and the mean intersection over union (mIoU) of this mitral valve object detection model were 0.530 and 0.554, respectively. The detailed flow of this step is described below.

(1) The robot position is adjusted manually so that the initial position of the probe is at the subject's xiphoid process.

(2) The position (x-axis, y-axis) of the probe is moved to execute a three-way traveling scan on the left chest wall (see **Fig. 6**). The US images with the probe position information are collected along the path. Note that the angle of the probe is fixed at 0° for roll, yaw, and pitch, respectively as the initial value of the rotation. The scan range shown in **Fig. 6** was determined experimentally.

(3) The mitral valve is detected in each acquired US image using YOLOv7 as the object detection method.

(4) The image with the maximum confidence score for detecting the mitral valve is chosen from the mitral valve detection images. The probe is moved to the position at which the image with the max confidence score was obtained.

(5) The probe position is fixed at the position derived in (4) and US images are captured for 2 seconds, which is equivalent to the duration of two heartbeats. The continuity of mitral valve detection is evaluated in the acquired images to confirm that the position derived in (4) is the appropriate position to display the mitral valve. If not appropriate, repeat (5) at the position where the next highest mitral valve confidence score is obtained. Note that mitral valve detection is considered to be continuous if there are three consecutive images in which the mitral valve is detected out of 100 images (frame rate 50 Hz) during two heartbeats. The mitral valve is considered to be visible if the confidence score is greater than 0.25.

(6) If the continuity is confirmed, the probe position at which the mitral valve is displayed correctly can be estimated. If the above conditions are not satisfied, yaw is rotated by +15° and steps 2 to 5 are performed again. Note that if yaw becomes larger than +45°, the mitral valve is considered to be undetectable, and this process ends as an exception.

(7) The probe is moved to the position where the detected mitral valve is along the central axis of the US image. If the mitral valve is lost during the movement, move the probe to the position where the mitral valve is closest to the central axis in the acquisition.

C. Step2: Left Ventricular Long-Axis Angle Search

The goal of step 2 is to estimate the yaw angle of the probe parallel to the left ventricular long-axis. The interventricular septum and the US irradiation plane must be parallel; this is a condition for depicting the parasternal long-axis view. Furthermore, the interventricular septum is difficult to detect accurately because the interventricular septum does not move, unlike the mitral valve. This method then focuses on the left

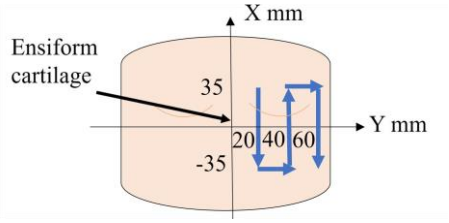

Fig.6. Trajectory of three-way travel scan on the left chest wall

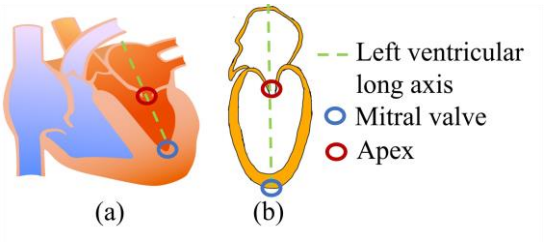

Fig.7. Left ventricular axis and left ventricle/atrium; (a) overview; (b) cross section

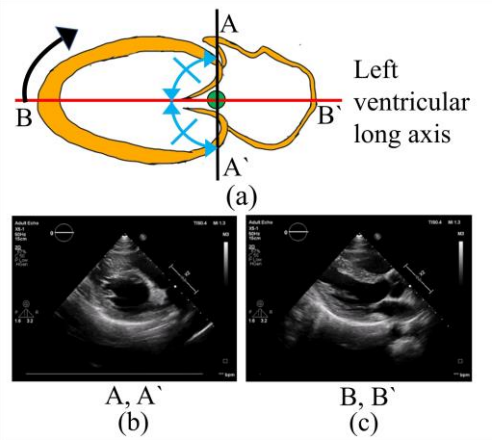

Fig.8. Symmetry of cross section to left ventricular axis and shape of left ventricular wall; (a) location of cross section on left ventricle and left atrium; (b) closed loop; (c) open loop

ventricular long-axis, which is parallel to the interventricular septum. The left ventricular long-axis is a straight line that connects the apex and the mitral valve of the heart (see **Fig. 7(a)**). Step 2 estimates the left ventricular long-axis and derives the yaw angle of the probe such that the US plane is parallel to the left ventricular long-axis.

Step 2 focuses on the shape of the left ventricle and left atrium of the heart. As the left ventricle and left atrium can be approximated as ellipsoids [21] and the left ventricle and left atrium are anatomically connected by an interventricular septum, the left ventricle and left atrium are assumed to be approximated together as a rotating ellipsoid. The central axis of the ellipsoid of revolution coincides with the left ventricular long-axis (see **Fig. 7(b)**). The symmetry of the rotating ellipsoid (see **Fig. 8(a)**) suggests that there exists a cross-section A´ that is symmetrical to the left ventricular longitudinal axis at the cross-section A passing through the focal point F on the left ventricular long-axis. The median value of the probe angle at which cross sections A and A´ are obtained coincides with the left ventricular long-axis.

The probe is rotated along yaw direction from the probe angle that can depict the left ventricular long-axis to focus on

the cross-section of the left ventricular wall. The shape of the left ventricular wall in the cross-section changes in the order of open loop, closed loop, open loop, and closed loop when the probe is rotated in the direction of the black arrow in **Fig. 8(a)** for yaw (see **Fig. 8(b), (c)**). The parasternal short-axis view at the level of the mitral valve (see **Fig. 9**) is the focus of attention. This view is at the center of the closed loop section and is obtained when the yaw angle is rotated ±90° from the left ventricular axis angle. First, this step derives the yaw angles for the two image groups including the parasternal short-axis view at the level of the mitral valve with high confidence scores calculated with the object detection model using YOLOv7. Next, the median yaw value for the two image groups is assumed to be the probe angle at which the left ventricular long-axis can be depicted. Note that the parasternal short-axis view at the level of the mitral valve was focused on for the following reasons among the group of US images obtained when the yaw angle was rotated: i) the feature is clear in the US image obtained when the yaw angle is rotated, and ii) the change in the US image is large relative to the change in yaw angle.

The detailed process for the above is described below. Note that the left ventricular region in the parasternal short-axis view at the level of the mitral valve was detected using YOLO v7. The left ventricular region in the parasternal short-axis view at the level of the mitral valve object detection model was trained using 1648 images for training and 413 images for validation. Images for training and validation were obtained from 7 males in their 20s. These images were acquired by adjusting the position and angle of the probe by hand and fulfilled the conditions for the parasternal short-axis view at the level of the mitral valve shown in **Fig. 9**. Annotation of the left ventricular wall in the training images is performed as shown in Fig.5(b). The number of epochs was 200 and the batch size was 8. The mAP50 and mIoU of the model used to detect the left ventricular region in the parasternal short-axis view at the level of the mitral valve were 0.998 and 0.883, respectively.

(1) The yaw angle is rotated from −180° to 180°. Note that the probe position (x-axis, y-axis) and angle (roll, pitch) are set to the value estimated in step 1.

(2) The left ventricular region in the parasternal short-axis view at the level of the mitral valve is detected in each acquired US image using the object detection method with YOLOv7.

(3) First, the angle of yaw rotation of the probe (−180° to 180°) is divided into sections of 3° each, and the sum of the confidence scores of the left ventricle are calculated for each section. The sum of the confidence scores within each segment is taken and compared to avoid misidentification of the location where the local peak of the confidence score was obtained as the parasternal short-axis view at the level of the mitral valve detection location. This allows identification of locations where the parasternal short-axis view at the level of the mitral valve can be detected with a regularly high confidence score. Next, the yaw angle showing the parasternal short-axis view at the level of the mitral valve is estimated to be the central angle of the top two intervals having the highest total left ventricular confidence score.

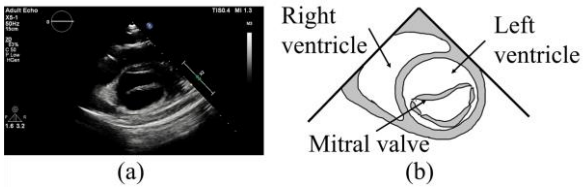

Fig.9. Parasternal short-axis view at the level of the mitral valve; (b) US image; (c) schematic depiction

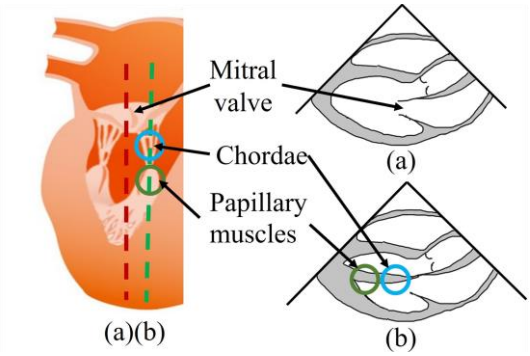

Fig.10. Position of tendon chordae and papillary muscles and Pitch angle of probe. (a) Pitch angle is appropriate. (b) Pitch angle is inappropriate.

(4) The left ventricular long-axis angle is estimated to be the median of the two angles that depict the parasternal short-axis view at the level of the mitral valve calculated in (3).

(5) The yaw angle of the probe is adjusted to the estimated left ventricular long-axis.

D. Step 3: Mitral Valve Angle Search

The goal of step 3 is to estimate the pitch angle of the probe with which it is possible to obtain US images in which the mitral valve is not connected to the papillary muscle or chordae. The mitral valve should not be connected to the papillary muscles or chordae of the left ventricle in the parasternal long-axis view, because if it were, the movement of the tip of the mitral valve could not be observed. Observing the movement of the mitral valve tip can confirm that the mitral valve is functioning properly, and that no regurgitation of blood is occurring. In the parasternal long-axis view that is displayed when the pitch angle of the probe is appropriately adjusted, the mitral valve is not connected to the chordae or papillary muscles (see **Fig. 10(a)**), but the mitral valve is connected to them when the pitch angle of the probe is not adjusted (see **Fig. 10(b)**). Next, we assume that the optimal pitch angle of the probe can be estimated by focusing on the visualized shape of the mitral valve in the obtained US image.

The mitral valve shape is recognized by the mitral valve detection system introduced in Section III B. In this system, the confidence scores of mitral valve are lower when the mitral valve is connected to chordae or papillary muscles than when the mitral valve is in the parasternal long-axis view. Then when the probe is rotated at the appropriate pitch angle, the shape of the visualized mitral valve is close to the annotated mitral valve in the training image. First, the pitch angle of the probe is varied to identify the pitch angle at which the maximum confidence score for the mitral valve detection is obtained. Next, this pitch angle is determined to be the

optimal pitch angle at which the parasternal long-axis view can be obtained. The detailed method is described below.
(1) Rotate the pitch angle from −10° to 10° and capture a US image with the angle information attached. Note that the probe position (x-axis, y-axis) and angles (roll, yaw) are fixed to the values estimated in step 2.
(2) The mitral valve is detected in each US image obtained using the object detection method with YOLOv7.
(3) The optimal pitch angle is determined to be where the mitral valve is detected with the maximum confidence score in the acquired images.

IV. Evaluation

A. Experimental Setup

The developed parasternal long-axis view search system was verified for i) each step of detection accuracy, and ii) total system detection accuracy. The experiments were performed using the developed echocardiographic robot and US equipment (EPIQ 7G, Philips, Netherlands). The subjects were six males. The height, weight, and BMI of the subjects are shown in **Table I**. This study was exempted from ethics application in accordance with the ethical standards of the Institutional Research Committee at Waseda University because the experiment was conducted to laboratory staff and students.

1) Verification of Detection Accuracy for Each Step

In this experiment, the accuracy of each step of the proposed parasternal long-axis view search method was evaluated quantitatively and was verified. The detailed procedure for the experiment is given below.
(1) Gel is applied to the subject's chest wall and the probe is moved to the xiphoid process, which is its initial position.
(2) The search for each step is performed. Note that a mitral valve position search is performed in step 1 (see Section III B), a left ventricular long-axis angle search is performed in step 2 (see Section III C), and a mitral valve angle search is performed in step 3 (see Section III D).
(3) (1) and (2) above are performed five times for each step of proposed method.
(4) The images at the end of each step are scored according to the evaluation criteria shown in **Table II**. The validity of the search is then verified based on the scores.

Note that steps 2 and 3 are performed after the probe is moved to a position where it can acquire an image that satisfies the evaluation criteria of the previous step shown in **Table II**.

2) Verification of Total System Detection Accuracy

The probability of detecting the parasternal long-axis view is verified in this experiment when all the steps of the proposed search system are performed consecutively as the total system. Then, the validity of the total system is verified based on the probability of detecting the paraste rnal long-axis view. The results are compared with those of Section IV A-1 to identify the issues that arise when the steps are combined. The detailed experimental procedure is given below.
(1) Gel is applied to the subject's chest wall and the probe is moved to the xiphoid process, which is its initial position.

TABLE I. Height, Weight, and BMI of Each Subject

subject	height cm	weight kg	BMI kg/m^2
A	157	50.4	20.4
B	170	57.5	19.9
C	170	64.0	22.1
D	170	60.0	20.8
E	171	54.0	18.5
F	175	75.5	24.7

TABLE II. Image Conditions to be Explored in Each Step

	Evaluation criteria
Step 1	• Mitral valve can be observed.
Step 2	• Left ventricular wall is open loop. • Anterior aortic wall higher than interventricular septum.
Step 3	• The tip of the mitral valve is not connected to the chordae or papillary muscle. • Left ventricle, mitral valve and aortic valve can be observed.
Total	• Left ventricular wall is open loop. • Anterior aortic wall higher than interventricular septum. • The tip of the mitral valve is not connected to the chordae or papillary muscle.

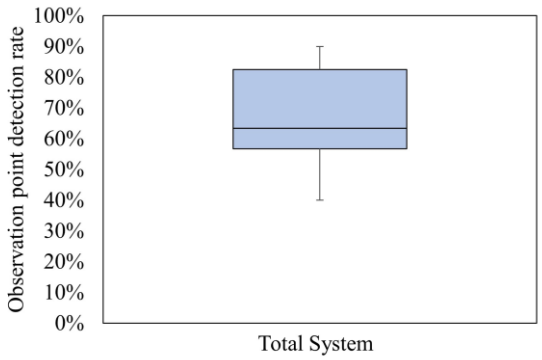

Fig.11. Box-and-whisker plot of the observation point detection rate for all trials

(2) The proposed search for the parasternal long-axis view is performed continuously for all steps.
(3) (1) and (2) above are performed five times.
(4) The images at the end of the search are scored according to the evaluation criteria shown in **Table II**. The validity of the method is verified based on these scores. Note that each condition is scored as 1 point: 1 point should be given for each site that can be observed in Table II under the heading "Left ventricle, mitral valve, and aortic valve can be observed.".

B. Results

1) Verification of Each Step Detection Accuracy

Table III shows the number of times that each condition shown in **Table II** was satisfied by the images detected during the search for each step for each subject. Note that the

TABLE III. NUMBER OF TIMES THE CONDITION WAS DETECTED IN EACH STEP VALIDATION TEST FOR THE SUBJECTS

subject	Step1		Step2	Step3
	mitral valve	open loop	anterior wall of aorta and interventricular septum	papillary muscles and chordae
A	4/5	**2/5**	3/5	**2/5**
B	5/5	4/5	3/5	4/5
C	5/5	4/5	4/5	4/5
D	5/5	3/5	**1/5**	5/5
E	**2/5**	**1/5**	**2/5**	5/5
F	3/5	5/5	**1/5**	4/5
total	24/30	19/30	**14/30**	24/30

TABLE IV. NUMBER OF TIMES THE CONDITION WAS DETECTED IN TOTAL SYSTEM VALIDATION TEST FOR THE SUBJECTS

subject	left ventricle	mitral valve	aortic valve	open loop	anterior wall of aorta and interventricular septum	papillary muscles and chordae	total points	search time min
A	**2/5**	4/5	3/5	**2/5**	4/5	**2/5**	17/30	3.62
B	5/5	5/5	4/5	5/5	3/5	5/5	27/30	3.78
C	5/5	5/5	3/5	5/5	3/5	5/5	26/30	3.82
D	4/5	5/5	4/5	**2/5**	3/5	3/5	21/30	5.05
E	**1/5**	3/5	**2/5**	**2/5**	**2/5**	**2/5**	**12/30**	4.23
F	4/5	4/5	3/5	**2/5**	**2/5**	**2/5**	17/30	3.63
total	21/30	26/30	19/30	18/30	17/30	19/30	120/180	4.02

boldface numbers indicates that the condition was satisfied less than twice. The validation for subject E for step 2 failed to acquire an image that satisfied the evaluation criteria for the previous step shown in **Table II** two out of five times.

2) Verification of Total System Detection Accuracy

Table IV shows the number of times that each condition shown in "Total" in **Table II** was satisfied by the images detected during the total system verification with the subjects and the total system search time. Note that boldface numbers indicate that less than 40% of the total number of trials satisfied the conditions. **Fig. 11** shows a box-and-whisker plot of the observation point detection rate for all trials.

C. Discussions

1) Verification of Each Step Detection Accuracy

The evaluation conditions were satisfied in the majority of the 30 trials in each step (see **Table III**). However, for subject A the system could not satisfy the condition in which the left ventricular wall is an open loop in 2 out of 5 trials in step 2. In step 3, the tip of the mitral valve was not connected to the tendinous and papillary muscles in 2 of 5 trials. For subject D and F, the system was able to obtain an image of the anterior aortic wall higher than the interventricular septum in only 1 out of 5 trials in step 2. For subject E, the system was only able to observe the mitral valve in 2 out of 5 trials in step 1. The condition in which the left ventricular wall is open was satisfied only in 1 trial, and the condition in which the anterior aortic wall is higher than the interventricular septum was satisfied in 2 of the 5 trials in step 2. These results might have been caused by idiosyncratic reasons for each subject, and we analyze them next.

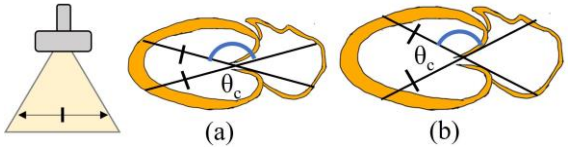

Fig.12. Heart size and closed-loop angle (a) with small heart; (b) with large heart

Subject A is the shortest of the subjects in height (see **Table I**). Thus, the size of the subject's heart is assumed to be smaller than that of the other subjects. The left ventricular wall becomes a closed loop when the left ventricular wall fits within the range displayed by the probe. The closed loop angle θ_c may vary depending on the size of the heart, as shown in **Fig. 12**. Thus, more images are obtained closer to the parasternal short-axis view at the level of the mitral valve in the images acquired in step 2 when the heart is smaller. This may increase the possibility of false positives. This problem can be solved by conducting a step 2 search using an object detection model for small subjects trained only on the parasternal short-axis view at the level of the mitral valve images, which contains more circular left ventricular wall features than the object detection model used in this paper.

It is assumed that for subject D and F, the system could not obtain an image in which the anterior or aortic wall was higher than the interventricular septum at a position parallel to the left ventricular long-axis. Step 2 was constructed based on the hypothesis that images that depict the anterior aortic wall higher than the interventricular septum are obtained when the yaw of the probe is parallel to the left ventricular long-axis. However, it is possible that there are subjects for whom this assumption does not hold, such as subject D. The necessary observation points can be divided into two types, depending

on the disease to be diagnosed: i) to observe the width of the left ventricle using an image of the open ring of the left ventricular wall, ii) to observe the anterior aortic wall and interventricular septum. The former of the above two observations is covered in this study, but the latter is not. Therefore, it is necessary to construct a search method that can manage the latter of the above two observation points as well and change the method according to the disease to be diagnosed.

Subject E has a low BMI and a thin body type (see **Table I**). The distance between the costal bones and the skin is closer in the thin type than in the normal body shape due to the difference in tissue thickness. The costal bones interfere with the echoes and generate shadows. Thus, the angle at which the echoes are obstructed is larger for the thin body type than for the normal body type, and this may make detection more difficult (see **Fig.13**). On the other hand, subject E had low detection accuracy for steps 1 and 2, but high detection accuracy for step 3. This is assumed to be due to the relationship between the US radiation plane and the placement of the costal bones. The costal bones are perpendicular to the US radiation plane in yaw rotation (see **Fig.14(a)**). In contrast, the costal bones are parallel to the US radiation plane in pitch rotation (see **Fig. 14(b)**). For this reason, it is assumed that US waves are less likely to be blocked by the costal bones in the pitch rotation than in the yaw rotation. Thus, the accuracy of step 3 was considered to be high, even for a thin body type. To address the issue, we may require an estimation method for detecting artifacts and removing US images that show a large effect of artifacts for thin body types. The position estimated in step 1 in thin body types may have a large effect on bone artifacts. In this case, the probe is moved to the next position with the next highest mitral valve confidence score. The search is resumed if the new location shows less effect from the costal bones and the mitral valve is detectable. It is considered necessary to repeat this process to estimate the appropriate location with the least effect from the costal bones. In addition, in step 2, although we applied the noise processing in the estimation method described in Section III-C, other noise reductions such as low-pass filtering may be applicable for improving further the estimation accuracy.

2) Verification of Total System Detection Accuracy

The observation point detection rate was 63.3 ± 5.3 % at the median after 30 trials for the method proposed in this paper (see **Fig. 11**). As shown in **Table IV**, even if the observation point is not obtained in the previous step, it may be obtained in a later step in some cases. This suggests that each of the steps might have complemented each other, and the final estimation accuracy might not have been significantly affected even if the detection results of the previous step were not able to estimate the optimal location.

On the other hand, the number of observations of some features was relatively low for subjects A, D, E and F, as in the result of the first experiment. For subject E, the detection accuracy in steps 1 and 2 was low, as shown in the result of the first experiment. Then, the accuracy of step 3 was further reduced because step 3 is based on the performance of steps 1 and 2 when each step is conducted consecutively in the total system.

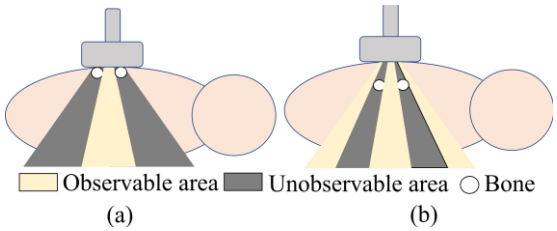

Fig.13. Effect of costal bones on US acquisition; (a) thin body type; (b) normal body type

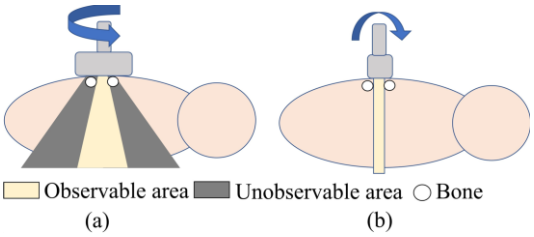

Fig.14. Probe rotation angle and costal bones influence; (a)Yaw; (b) Pitch

The average test time for the total system was 4.02 ± 0.5 minutes. A general echocardiography examination takes about 40~60 minutes [22]. Echocardiography involves obtaining multiple views of the heart and integrating the information obtained from these views to confirm the shape and motion of the heart and to diagnose the presence or absence of disease. Thus, the time required to obtain the parasternal long-axis view is considered to be about a few minutes in the examination time. It is necessary to measure and compare the time required for physicians to acquire the parasternal long-axis view to determine whether the examination time using the proposed method is appropriate for actual use in the medical field. We are planning to do this in cooperation with physicians in the future.

D. Limitations

There are several limitations of the developed search method. Since the search method was developed based on the healthy subjects, it may be difficult to apply the subjects with significant abnormalities in the shape of the mitral valve, left ventricle, or left atrium. This problem may be solved by using an object detection model that learns the shape of abnormal parts caused by disease. Also, in step 1, the range of exhaustive search was determined experimentally, and in step 2, the left atrium and left ventricle of the heart are approximated together as an ellipsoid. Meanwhile, it is unclear whether the range of Step 1 and the ellipsoid approximation of Step 2 are appropriate for all patients. In the future, it is necessary to conduct tests on a large number of subjects to verify the validity of the search area and the validity of elliptical approximation of the left atrium and left ventricle together.

Although we mentioned the difficulty of searching for a parasternal long-axis view in thin body types, there was only one thin-type subject in this study. Therefore, it is necessary to implement the proposed method on a larger number of thin-type subjects and further analyze issues related to the thin

bodies. Also, no obese and female subjects were tested in this study. It is known that for obese and female subjects, fat must be avoided or compressed by adjusting the pressure applied to the probe to search for and acquire images. It is necessary to combine this exploratory method with a probe pressure-adjusted approach for those subjects.

The recognition accuracy of the mitral valve with YOLOv7 was low. This may be due to the fact that the mitral valve is a region of significant motion. For example, there is a difference in the characteristics of the mitral valve when it is most open and when it is in the process of opening, even when the mitral valve is annotated according to the criteria described in Section III B. We assumed that the number of images for each condition was not enough, and that the learning accuracy could not be ensured. It is necessary to improve the recognition accuracy by preparing the number of images considered appropriate for learning for each mitral valve opening condition.

The evaluation of US images using the proposed method was performed with clear observation points and objectivity, but the evaluation was not performed by physicians. In the future, it will be necessary to have physicians evaluate the images acquired by the search to determine whether they are diagnostic or not.

V. Conclusion

This study proposes a method for estimating the position and angle of the acoustic window that enables the acquisition of a parasternal long-axis view by an echocardiography robot. The proposed method consists of three steps: i) mitral valve position search, ii) left ventricular long-axis angle search, and iii) mitral valve angle search. Each step identifies i) the x-axis and y-axis from where the mitral valve appears in the center, ii) the yaw parallel to the left ventricular long-axis, and iii) the pitch where the mitral valve is not connected to the papillary muscle and chordae. The proposed method was validated on six subjects, and the median observation point detection rate was 63.3 ± 5.3%. These results suggest the validity of the proposed method. In the future, we plan to combine this method with an automated disease detection method by using the parasternal long-axis view and applying it to automated echocardiographic examinations by an echocardiography robot.

References

[1] WHO (World Health Organization), “Cardiovascular diseases (CVDs),” 2021, https://www.who.int/news-room/fact-sheets/detail/cardiovascular-diseases-(cvds), Accessed 30 January 2023

[2] Ministry of Health, Labour and Welfare,“Trends in death rates for leading causes of death,”2020.

[3] T. Y. Fang, H. K. Zhang, R. Finocchi, R. H. Taylor, and E. M. Boctor, “Force-assisted ultrasound imaging system through dual force sensing and admittance robot control,” Int. J. Comput. Assist. Radiol. Surg., vol. 12, no. 6, pp. 983–991, 2017.

[4] S. Wang, D. Singh, D. Johnson, K. Althoefer, "Robotic Ultrasound: View Planning, Tracking, and Automatic Acquisition of Transesophageal Echocardiography,” IEEE Robot. Autom. Mag., vol. 23, no. 4, pp. 118–127, 2016.

[5] R. Tsumura, J. W. Hardin, K. Bimbraw, A. V. Grossestreuer, O. S. Odusanya, Y. Zheng, J. C. Hill, B. Hoffmann, W. Soboyejo and H. K. Zhang, “Tele-Operative Low-Cost Robotic Lung Ultrasound Scanning Platform for Triage of COVID-19 Patients,” IEEE Robotics and Automation Letters, vol. 6, issue. 3, pp. 4664–4671, 2021

[6] R. Tsumura and H. Iwata, “Robotic fetal ultrasonography platform with a passive scan mechanism,” International Journal of Computer Assisted Radiology and Surgery, vol. 15, pp. 1323–1333, 2020

[7] Y. Shida, R. Tsumura, T. Watanabe and H. Iwata, "Heart Position Estimation based on Bone Distribution toward Autonomous Robotic Fetal Ultrasonography,”2021 IEEE International Conference on Robotics and Automation, paper no.940, 2021

[8] Y. Takachi, K. Masuda, T. Yoshinaga and Y. Aoki, "Development of a Support System for Handling Ultrasound Probe to Alleviate Fatigue of Physician by Introducing a Coordinated Motion with robot,”, Journal of the Robotics Society of Japan, vol. 29, no. 7, pp.634–642, 2011.

[9] M. Giuliani, D. Szczęśniak-Stańczyk, N. Mirnig, G. Stollnberger, M. Szyszko, B. Stańczyk and M. Tscheligi, “User-centred design and evaluation of a tele-operated echocardiography robot”, Health and Technology, vol. 10, pp.649-665, 2020

[10] Y. Shida, M. Sugawara, R. Tsumura, H. Chiba, T. Uejima and H. Iwata, “Diagnostic Posture Control System for Seated-Style Echocardiography Robot,” International Journal of Computer Assisted Radiology and Surgery, vol 18, issue. 3, 2023

[11] P. Zhu and Z. Li, “Guideline-based learning for standard plane extraction in 3-D echocardiography,” Journal of Medical Imaging, Vol. 5, Issue 4, 2018

[12] S. Dong, G. Luo, K. Wang, S. Cao, Q. Li, and H. Zhang, “A Combined Fully Convolutional Networks and Deformable Model for Automatic Left Ventricle Segmentation Based on 3D Echocardiography,” Biomed Res Int. 2018, 2018

[13] M. A. Degel, N. Navab and S. Albarqouni, “Domain and Geometry Agnostic CNNs for Left Atrium Segmentation in 3D Ultrasound,” 21st International Conference on Medical Image Computing and Computer Assisted Interventions (MICCAI), 2018

[14] Y. Huang, W. Xiao, C. Wang, H. Liu, R. Huang and Z. Sun, “Towards Fully Autonomous Ultrasound Scanning Robot With Imitation Learning Based on Clinical Protocols” IEEE Robotics and Automation Letters vol. 6, issue.2, pp.3671-3678, 2021

[15] R. Nakadate, J. Solis, A Takanishi, E Minagawa, M. Sugawara, K. Niki,” Out-of-plane visual servoing method for tracking the carotid artery with a robot-assisted ultrasound diagnostic system” 2011 IEEE International Conference on Robotics and Automation, 2011

[16] J. Zhou, N. Koizumi, Y. Nishiyama, K. Kogiso, T. Ishikawa, K. Kobayashi, Y. Watanabe, T. Fujibayashi, M. Yamada, M. Matsuyama, H. Tsukihara, R. Tsumura, K. Yoshinaka, N. Matsumoto, M. Ogawa, H. Miyazaki, K. Numata, H. Nagaoka, T. Iwai and H. Iijima, “A VS ultrasound diagnostic system with kidney image evaluation functions” Int J Comput Assist Radiol Surg. vol. 18, issue.2, pp.227-246, 2023.

[17] J. Zielke, C. Eilers, B. Busam, W. Weber, N. Navab, and T. Wendler, “RSV: Robotic Sonography for Thyroid Volumetry” IEEE Robotics and Automation Letters vol. 7, issue.2, pp.3342-3348,2022

[18] Z. Jiang, Y. Gao, L. Xie and N. Navab, “Towards Autonomous Atlas-Based Ultrasound Acquisitions in Presence of Articulated Motion” IEEE Robotics and Automation Letters vol. 7, issue.3, pp.7423-7430,2022

[19] Japanese Society of Sonographers, “Parasternal Long axis view,” 2023, https://www.jss.org/english/standard/standardization_ca/parasternal_long_axis_view.html, Accessed 30 January 2023

[20] C. Y. Wang, A. Bochkovskiy, H. Y. M. Liao, “YOLOv7: Trainable bag-of-freebies sets new state-of-the-art for real-time object detectors,” arXiv, 2022

[21] R. M. Lang, L. P. Badano, V. Mor-Avi, J. Afilalo, A. Armstrong, L. Ernande, F. A. Flachskampf, E. Foster, S. A. Goldstein, T. Kuznetsova, P. Lancellotti, D. Muraru, M. H. Picard, E. R. Rietzschel, L. Rudski, K. T. Spencer, W. Tsang, J. Voigt “Recommendations for Cardiac Chamber Quantification by Echocardiography in Adults: An Update from the American Society of Echocardiography and the European Association of Cardiovascular Imaging” European Heart Journal - Cardiovascular Imaging, 2015

[22] Cleveland Clinic, “Echocardiogram”, 2022, https://my.clevelandclinic.org/health/diagnostics/16947-echocardiogram, Accessed 12 April 2023